Self-Matching Assembly of Chiral Gold Nanoparticles Leads to High Optical Asymmetry and Sensitive Detection of Adenosine Triphosphate

Ning-Ning Zhang,[†,⊥] *Mikhail Mychinko,*[#] *Shu-Yang Gao,*[†] *Linxiuzi Yu,*[†] *Zhi-Li Shen,*[†] *Liang Wang,*[†] *Fei Peng,*[†] *Zhonglin Wei,*[∥] *Zizhun Wang,*[△] *Wei Zhang,*[△] *Shoujun Zhu,*[†,‡] *Yang Yang,*[†] *Tianmeng Sun,*[†,⊥] *Luis M. Liz-Marzán*[*,§,◇,□,▽], *Sara Bals*[*,#], *Kun Liu*[*,†,‡]

[†] State Key Laboratory of Supramolecular Structure and Materials, College of Chemistry, Jilin University, Changchun 130012, China

[⊥] Key Laboratory of Organ Regeneration and Transplantation of Ministry of Education, Institute of Immunology, The First Hospital, Jilin University, Changchun 130012, China

[#] EMAT and NANOlab Center of Excellence, University of Antwerp, 2020 Antwerp, Belgium

[∥] Department of Organic Chemistry, College of Chemistry, Jilin University, Changchun 130012, China

[△] Electron Microscopy Center, and Jilin Provincial International Cooperation Key Laboratory of High-Efficiency Clean Energy Materials, Key Laboratory of Automobile Materials MOE, Jilin University, Changchun 130012, China

[‡] Joint Laboratory of Opto-Functional Theranostics in Medicine and Chemistry, The First Hospital, Jilin University, Changchun 130012, China

[§] CIC biomaGUNE, Basque Research and Technology Alliance (BRTA), 20014 Donostia-San Sebastián, Spain

[◇] Ikerbasque, Basque Foundation for Science, 43009 Bilbao, Spain

[□] Networking Biomedical Research Center on Bioengineering, Biomaterials and Nanomedicine (CIBER-BBN), 20014 Donostia-San Sebastián, Spain

[▽] Cinbio, University of Vigo, 36310 Vigo, Spain

KEYWORDS: chirality, chiral assembly, gold nanorods, plasmonics, ATP detection

ABSTRACT. To achieve chiral amplification, life uses small chiral molecules as building blocks to construct hierarchical chiral architectures that can realize advanced physiological functions. Inspired by the chiral amplification strategy of nature, we herein demonstrate that the chiral assembly of chiral gold nanorods (GNRs) leads to an enhancement of optical asymmetry factors (g-factors), up to 0.24. The assembly of chiral GNRs, dictated by their structural self-matching, induced g-factors with over 100-fold higher values than that of individual chiral GNRs, in agreement with numerical simulations. Additionally, the enhanced g-factor of chiral GNR assemblies allowed their use as highly sensitive sensors of adenosine triphosphate (ATP detection limit of 1.0 μM), with selectivity against adenosine diphosphate and adenosine monophosphate.

Chirality is a crucial signature of living systems.[1] At the molecular scale, chirality is amplified by hierarchical self-assembly, to form dynamic chiral structures across multiple length scales, from genes through cells, embryos, to vessels and even organs.[4-7] A significant effort has been devoted to chiral self-assembly using artificial building blocks, including chiral molecules and achiral nanoparticles (NPs). A variety of fascinating chiral structures at multiple scales have been fabricated from chiral molecules, but chiral amplification of their chiroptical signals could hardly be achieved, due to the small interaction cross-sections between molecules and light.[8,9] In contrast, the much higher polarizability of plasmonic and semiconductor NPs leads to a substantial increase in the strength of chiroptical activity, i.e., optical asymmetry *g*-factors.[10-22] High *g*-factors have also been achieved by growing plasmonic NPs with well-defined chiral morphologies, i.e. chiral NPs.[23-32] So far, chiral assembly has however been restricted to achiral NP building blocks with rare exceptions.[23] We hypothesized that the use of chiral NPs as building blocks for chiral assemblies–mimicking the strategy in biological systems–might lead to further amplification of the chiroptical activity.

Chiroplasmonic nanostructures enable the amplification and transfer of the chiral signals of biomolecules, which can be used to enhance the sensitivity of chiral biomolecule detection.[13] Adenosine triphosphate (ATP) is an important biomolecule because it serves as the energy source for most biological functions, while playing a major role in extracellular signaling and DNA replication.[34-37] Detection methods based on chiroplasmonic nanostructures have been rarely explored,[38-40] they offer the possibility to achieve highly sensitive and selective ATP detection.

Herein, we report the hierarchical assembly of chiral gold nanorods (c-GNRs) into chiral superstructures, mimicking biological hierarchical self-assembly and leading to unusually high optical asymmetry. The helical morphology of chiral GNRs (c-GNRs) generates a structural self-

matching effect based on side-by-side assembly. Chiral assembly was achieved when using c-GNRs as the building units and achiral salts as inducers, resulting in higher-order chiral nanostructures with a remarkable enhancement of the optical asymmetry and *g*-factor values up to 0.24. Using finite-difference time-domain (FDTD) electromagnetic simulations, we explored the key factors leading to such a high chiroptical response in c-GNR assemblies. Based on the high optical activity of c-GNR assemblies, we demonstrate highly sensitive and selective detection of ATP, ADP, and AMP in physiological environments.

Both enantiomers of c-GNRs were prepared by seeded-growth on single-crystalline achiral GNRs, in the presence of L-/D-Cysteine (L-/D-Cys) as chiral inducer, following a previously reported method (Figure 1).[41] As shown by scanning electron microscopy (SEM) images (Figure 1A,D), L-/D-Cys-induced c-GNRs displayed right-/left-handed twisted structures, so we denote them as right-/left-handed helical GNRs (RH-/LH-GNRs), respectively. SEM image analysis revealed that LH-/RH-GNRs possess an average length of 54.2±2.9/53.9±1.5 nm, an average diameter at the central part of 15.3±0.6/15.5±0.6 nm, and an average diameter at the ends of 20.2±0.8/20.8±0.9 nm, respectively. The smaller diameter at the center of RH-/LH-GNRs suggested a concave shape of the c-GNR side-facets. These LH-/RH-GNRs exhibited almost identical extinction spectra but mirror-symmetrical CD spectra, with two CD bands, which we tentatively assigned to a transverse surface plasmon resonance (TSPR) at 540 nm and a longitudinal surface plasmon resonance (LSPR) at 750 nm, respectively (Figure 1G,H). The corresponding *g*-factor spectra of LH-/RH-GNRs also displayed nearly symmetric signals(Figure 1I), in good agreement with our previous report.**Error! Bookmark not defined.**

We employed electron tomography (ET) reconstructions to investigate the morphology of individual RH-/LH-GNRs in more detail. As shown in the ET reconstruction, the sides of c-GNRs

showed four twisted stripes, similar to a rounded rectangular prism upon torsional deformation along its long axis, resulting in concave side-faces (Figures 1B, E, and Movies S1,S2). The ET reconstructions further confirmed that the four twisted stripes of L/D-Cys GNRs were oriented in a right-/left-handed direction, respectively. From ET reconstructions, the helicity of c-GNRs could also be quantified, following a recently reported method.[42] From the calculated helicity functions $H(\rho,\alpha)$, a total helicity H_{total} value of +0.11 was determined for RH-GNRs (Figure 1C), indicating right-handedness, whereas that for LH-GNR (-0.17) indicates left-handedness (Figure 1F).

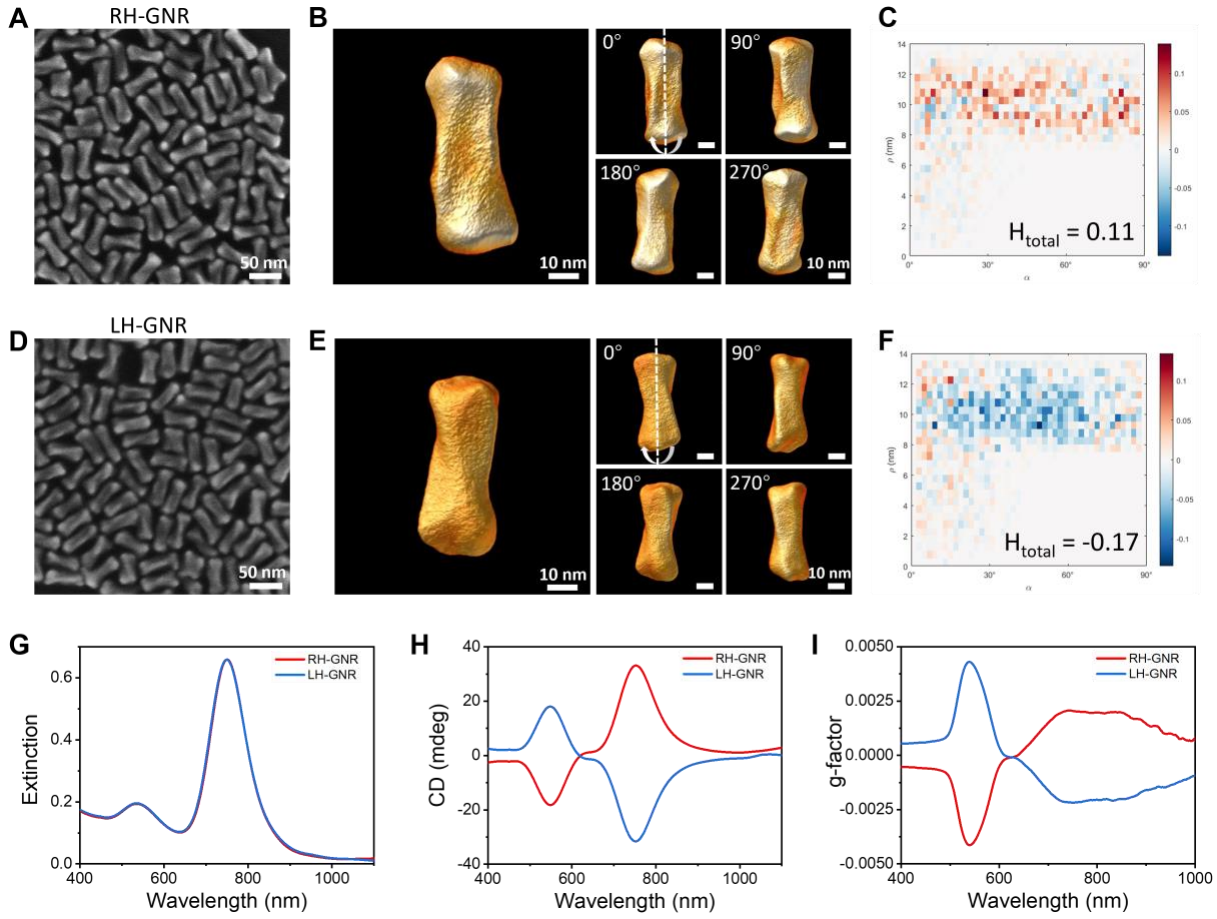

Figure 1. (A) SEM image and (B) visualizations of ET reconstructions of RH-GNRs, along with (C) a plot of the helicity function $H(\rho,\alpha)$ corresponding to (B). (D) SEM image and (E) visualizations of ET reconstructions of LH-GNRs, along with (F) a plot of the helicity function $H(\rho,\alpha)$ corresponding to (E). The red and blue colors in (C) and (F) indicate the presence of right-

and left-handed features, respectively; total helicity values are indicated in each plot. (G) Extinction, (H) CD, and (I) *g*-factor spectra of RH-/LH-GNRs, as labeled.

Unlike most chiral assemblies, where chiral molecular linkers direct the assembly of achiral NPs,[43-46] the twisted structure of c-GNRs in this work leads to mutual recognition and assembly, with no need for chiral linkers. We aimed at the electrostatic assembly of c-GNRs, induced by small molecular anions (Figure 2A).[47,48] We therefore tested anions with different numbers of COO^- groups to alter the surface charge of c-GNRs and, as a result, enhance electrostatic attraction. Upon addition of either sodium acetate or sodium malonate dibasic, the corresponding extinction spectra of c-GNRs (Figure S1) showed no observable changes of the peak position and intensity, indicating that anions with either one or two carboxyl groups cannot efficiently induce c-GNR self-assembly. In contrast, the addition of sodium citrate caused a significant blue shift of the LSPR band (from 753 to 727 nm) and a red shift of the TSPR (from 530 to 540 nm), suggesting that c-GNR self-assembly occurred in a side-by-side fashion (Figure 2B).[12,13] Zeta-potential measurements before and after the addition of the various anions showed that, for sodium acetate and sodium malonate dibasic, the zeta-potential decreased from +40.0 mV to +30.3 and +28.4 mV, respectively, whereas a substantial decrease of zeta-potential to +12.1 mV was recorded upon addition of sodium citrate (Figure S1). This result suggests that multivalent anions in sodium citrate can more effectively reduce the electrostatic repulsion between positively charged GNRs, leading to mutual attraction and resulting in side-by-side assembly.

The CD spectra of RH-GNR assemblies induced by sodium citrate exhibited a characteristic left-handed bisignate peak, whereas the CD bands recorded for LH-GNR assemblies were opposite to those for RH-GNR assemblies (Figure 2C). Notably, in both cases the sign of CD signals for c-

GNR assemblies was inverted compared to that for the corresponding individual c-GNRs. To explore the mechanism of chirality inversion, we built the models of left-handed (chirality inversion) and right-handed (chirality consistency) assembly of the RH-GNRs. The results suggest that, when c-GNRs assembled in a direction opposite to their own handedness, adjacent c-GNRs are locked into each other and achieve a self-matching structure (Figure S2A). In contrast, if the handed-ness of the c-GNRs is consistent with that of the assembly, the c-GNR ends hinder each other to produce a side-by-side assembly (Figure S2B). As a result, c-GNRs are assembled in achiral inverted and structural self-matching manner. Additionally, a significant increase in CD was observed for increasing sodium citrate concentrations, up to 0.12 mM, and reaching values up to 3000 mdeg, compared to 50 mdeg for individual c-GNRs (1.0 nM) (Figure 2C). Sodium citrate concentrations higher than 0.15 mM induced the formation of disordered GNR aggregates, resulting in smaller CD *g*-factors (Figure S3). For the ordered assemblies, optical asymmetry *g*-factors as high as 0.17 at 700 nm and -0.24 at 850 nm were reached (Figure 2D), which are about two orders of magnitude larger than those for individual c-GNRs.

The maximum *g*-factor achieved in the present study is substantially higher than those reported in the literature for chiral assemblies of achiral NPs (generally below 0.05).[43,44,51,52] The maximum *g*-factor value herein (0.24) is twice that previously reported for long-range ordered chiral assemblies of achiral GNRs (0.12).**Error! Bookmark not defined.** This result suggests that the assembly of NPs with chiral morphology as building blocks can significantly enhance the optical asymmetry of chiral nanostructures. Additionally, the CD and extinction spectra of c-GNR assemblies showed no change after 1 hour and minor changes after 1 day (Figure S4), meaning that a steady state was reached at this time.

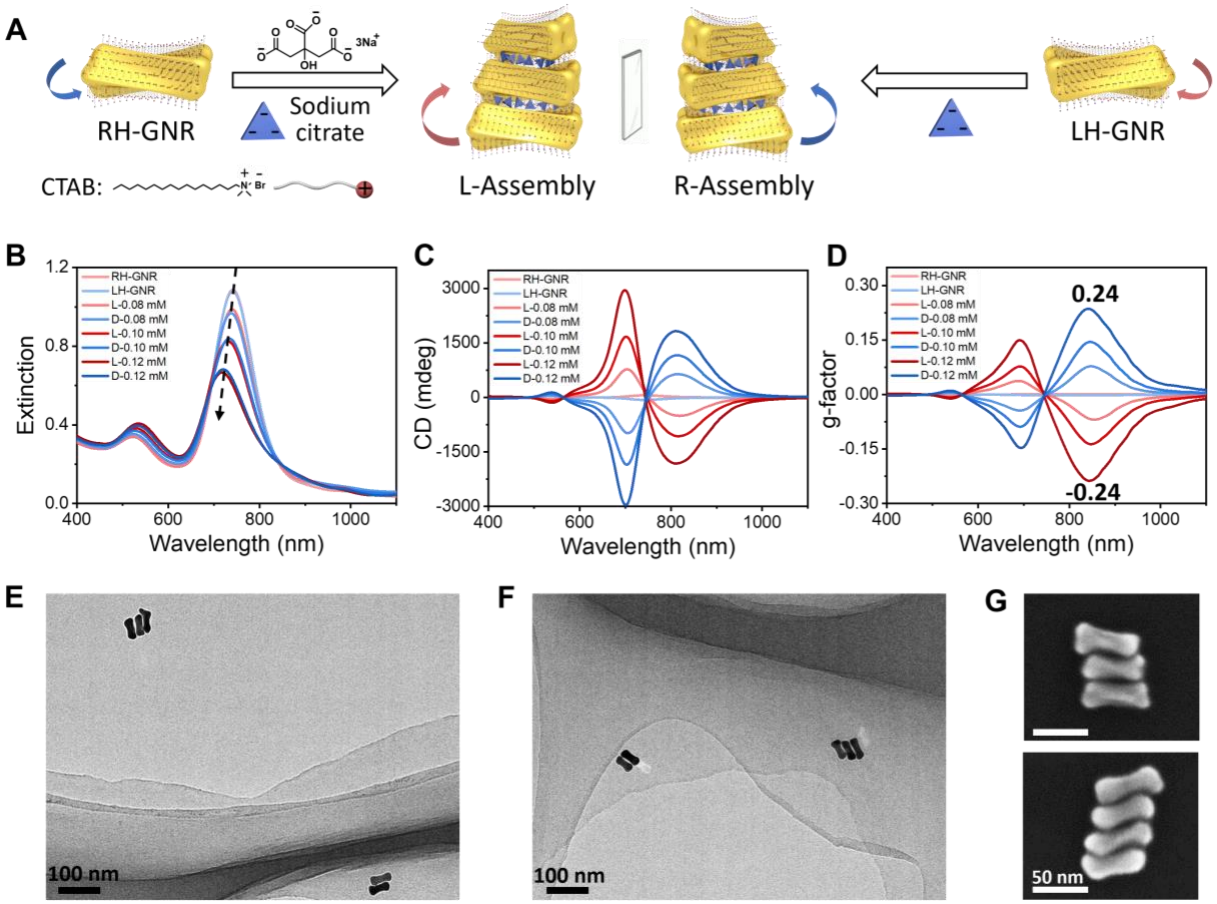

Figure 2. (A) Schematic diagram of the assembly of c-GNRs. (B-D) Extinction (B), CD (C), and *g*-factor (D) spectra for RH-/LH-GNRs assembled upon addition of sodium citrate at different concentrations (L/D in the caption represent L/D-assemblies). (E) Cryo-TEM images of RH-GNR assemblies. (F) Cryo-TEM image of LH-GNR assemblies. (G) SEM images of RH-GNR (top) and LH-GNR (bottom) assemblies. Even though the maximum CD value at 850 nm (1850 mdeg) is lower than the one at 700 nm (3000 mdeg), a higher g-factor at 850 nm results from a relative extinction intensity at 850 nm in the assemblies.

Next, we investigated in detail the structure of c-GNR assemblies by means of cryogenic transmission electron microscopy (Cryo-TEM), TEM, and ET reconstructions. Cryo-TEM images (Figure 2E,F) confirmed that assemblies were generated through side-by-side arrangement of c-GNRs in solution. SEM images (Figure 2G) additionally show side-by-side self-assembly. For ET

analysis, c-GNR assemblies formed by addition of 0.12 mM sodium citrate were stabilized by first capping with a thiol-ended hydrophobic ligand, 2-dipalmitoyl-sn-glycero-3-phosphothioethanol (sodium salt) and subsequently encapsulated by the amphiphilic block co-polymer poly(acrylic acid)-block-poly(styrene) (PAA-*b*-PS), as previously described.[11,53] Preservation of the assembly structure after encapsulation with PS-PAA was confirmed by the minor variations in the spectra of chiral assemblies, as shown in Figure S5. Polymer-coated assemblies were then separated by differential centrifugation, after which most of the assemblies were located in the middle gel layer, as shown in the inset of Figure 3A. TEM images of the assemblies taken from the middle layer showed side-by-side assembled structures, comprising 2 to 4 c-GNRs (Figure 3A,C), in agreement with the observed extinction spectra. The top and bottom layers of the centrifuged gel contained mainly isolated c-GNRs and large assembled structures, respectively (Figure S6). We additionally used silica encapsulation to capture c-GNR assemblies (Figures S5 and S7),[14] which further demonstrated the presence of c-GNR assemblies in solution (not upon drying and deposition on a substrate).

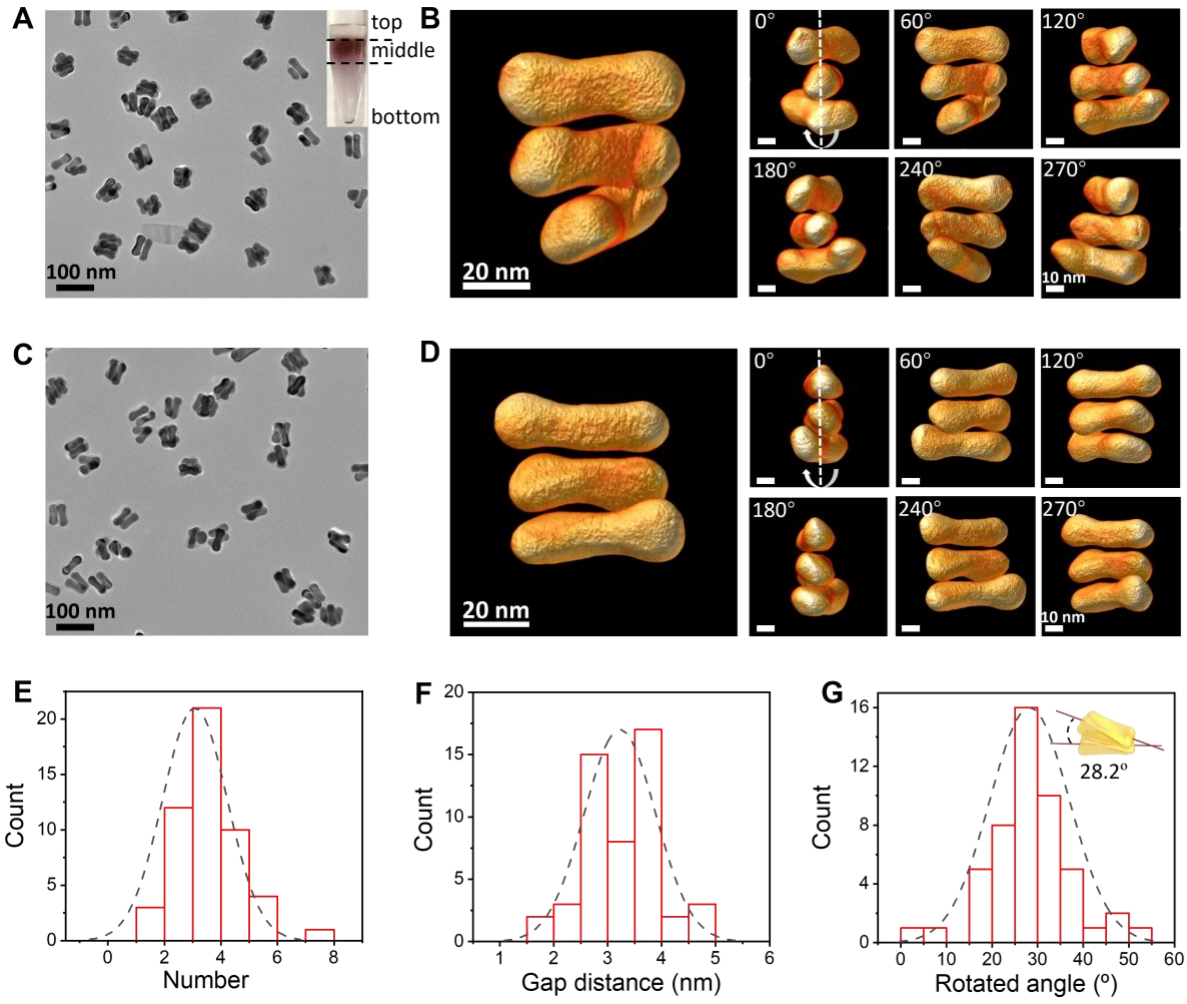

Figure 3. Chiral structures of c-GNR assemblies. (A) TEM image of polymer-coated RH-GNR assemblies. Shown in the inset is a photograph of polymer-coated assemblies after differential centrifugation. (B) 3D ET reconstructions of RH-GNR assemblies. (C) TEM image of polymer-coated LH-GNR assemblies. (D) 3D ET reconstructions of LH-GNR assemblies. (E) Statistical analysis of the assembled number of RH-GNRs. (F) Statistical analysis of gap distance between assembled RH-GNRs. (G) Statistical analysis of rotating angle in RH-GNR assemblies.

Statistical analysis of TEM images revealed average assembly numbers (*N,* the number of c-GNRs in each assembly) of 3.1±1.2 and 3.1±1.5, for RH- and LH-GNRs, respectively (Figures 3E and S8,S9). The average interparticle gap (*d*) in polymer-coated RH-GNR assemblies was

determined from 3D structures of ET reconstructions as 3.2±0.7 nm (Figures 3F and S10). Analysis of ET reconstructions of polymer-coated RH-GNR assemblies indicated an average rotation angle of 28.2±8.7° (Figures 3G and S10). To ensure accuracy, we performed statistical analysis on randomly selected samples(51, 50, and 50 samples for number, gap distance, and rotated angle analysis, respectively). The narrow distribution of gap distances and rotation angles (Figure 3F,G) confirmed the high uniformity of c-GNR assemblies.

Figure 3B,D and Movies S3,S4 show ET reconstructions of self-assembled structures for RH- and LH-GNRs. The ET reconstructions confirmed that RH-/LH-GNRs were assembled into left-/right-handed side-by-side helical structures, in agreement with the sign of chirality in the corresponding CD spectra (Figure 2C). As shown in Figure 3B/D, RH-GNRs/LH-GNRs were assembled through close contact of their twisted concave side-facets with structural self-matching, whereas the two adjacent GNR ends with relatively larger diameters were forced to be arranged in a non-parallel configuration (misaligned), resulting in the adjacent c-GNRs locking onto each other. It has been recently reported that chiral gold nanoarrows can assemble into orientated dimers by using a DNA origami template,[55] whereas dog-bone-shaped nanorods can generate assemblies through either electrostatic or hydrophobic interactions.[2,56] In the present work, we take this process a step further by achieving these assemblies with structural self-matching between the c-GNR building blocks. Control experiments (see Figure S11 for details) confirmed that the high g-factor c-GNR assemblies originates from the structure of self-matching of c-GNR assemblies, without any meaningful contribution from Cys ligands.

To better understand the chiroptical signals, we carried out FDTD simulations for both individual c-GNRs and their assemblies. The results from ET reconstructions of individual c-GNRs (Figure 1B,E) could be used as realistic models to simulate the extinction and CD spectra

(Figure S12), showing an agreement with the corresponding experimental spectra (Figure 1G,H). We additionally simulated the electric field enhancement distributions for c-GNRs, under both left circularly polarized (LCP) and right circularly polarized (RCP) light, at the wavelengths of LSPR and TSPR in the extinction spectra, respectively. The near-field enhancement maps showed asymmetric electric field distributions on c-GNRs, with distinct patterns under LCP and RCP (Figure S12A-D), indicating that the plasmonic chiroptical response of c-GNRs arises from their twisted structures. In addition, we constructed idealized c-GNR models and simulated their chiroptical properties (Figure S12E-H), with results that were also consistent with the experimental data (Figure 1G). Compared to the ET reconstruction models, the simulated LSPR position of idealized model matched the experimental results better. We found that the morphology of c-GNR tips strongly affect their LSPR position. Therefore, we hypothesize that there is diversity of tip morphology in the c-GNR sample, so that the c-GNR structures we imaged by ET does not sufficiently represent the overall sample in this case. The simulated extinction, CD, and *g*-factor spectra of RH-/LH-GNR assembly models were consistent with the corresponding experimental results, regarding peak positions and handedness (Figure S13).

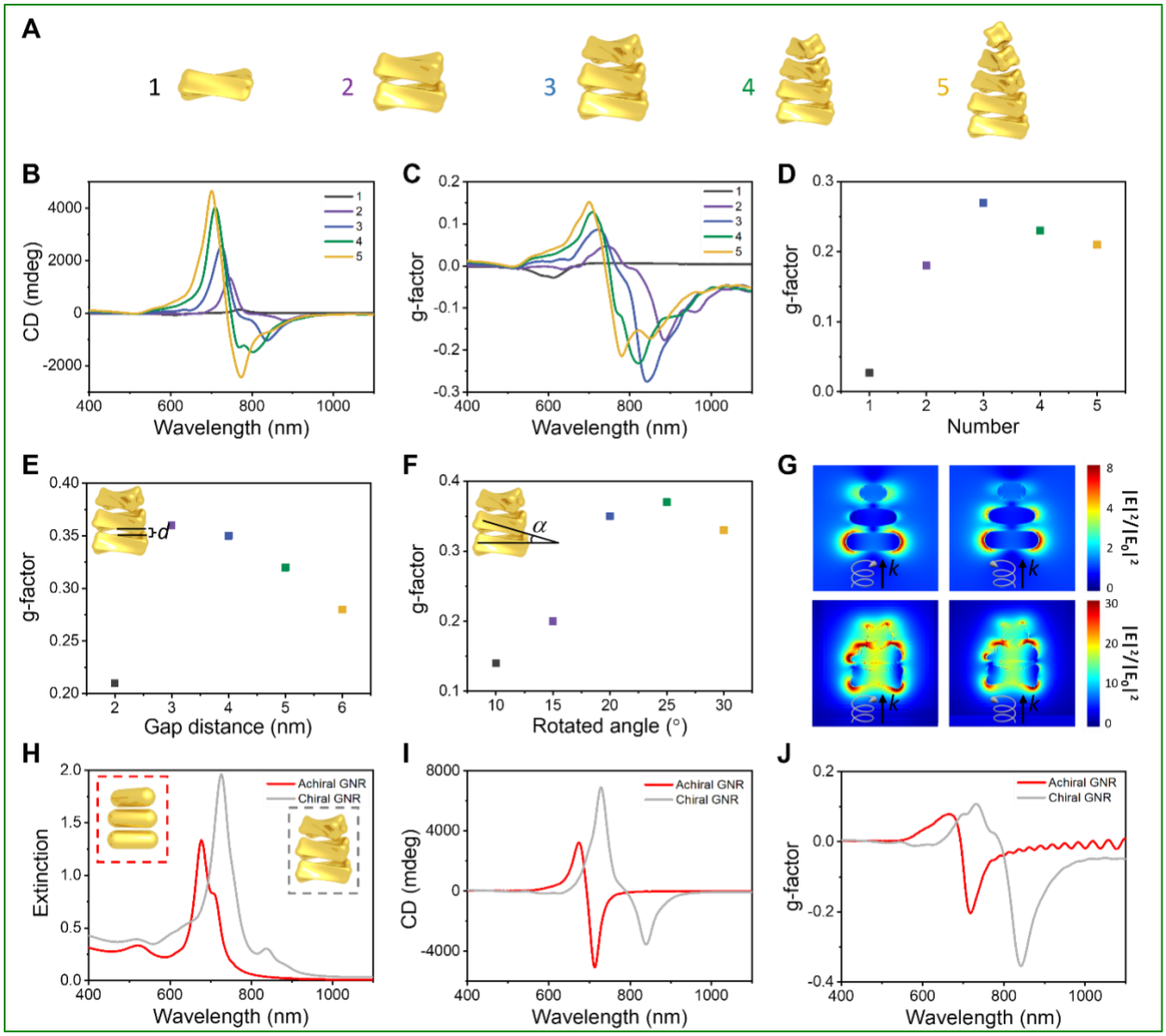

Figure 4. FDTD simulation of c-GNR assemblies. (A-C) Simulation models (A), CD spectra (B), and *g*-factor spectra (C) for assemblies with different number of RH-GNRs. (D) Plot of calculated *g*-factors for RH-GNR assemblies with different c-GNR number. (E) Variation of *g*-factor with the gap distance between adjacent RH-GNRs. (F) Variation of *g*-factor with the rotation angle between adjacent RH-GNRs. (G) Electric-field enhancement maps for achiral (top) and chiral (bottom) assemblies under irradiation with LCP (left) and RCP (right). (H-J) Extinction (H), CD (I), and *g*-factor (J) spectra for chiral assemblies made of achiral (red lines) and chiral (grey lines) GNRs.

We simulated next the optical properties of (idealized) RH-GNR assemblies with different N (Figure 4A). The extinction spectra showed gradually blue-shifting LSPR peaks with increasing N, from 1 to 5 (Figure S14A). Upon normalization by N, the simulated extinction spectra were consistent with the time-resolved extinction spectra during the assembly process(Figure 2B and Figure S14B). A distinct left-handed bisignate signal emerged in the CD band, with a positive peak at 520 nm and a negative peak at 750 nm. As N was increased, the CD signal at the LSPR band was gradually blue-shifted and enhanced, whereas the TSPR CD signal was gradually red-shifted and merged into the LSPR CD signal. The simulated CD spectra show substantially increased intensities of the CD signal with increasing N (Figure 4B), from 140 to 1400 mdeg for N of 1 and 2, respectively. The simulated g-factor spectra showed values reaching −0.27 at 842 nm for N = 3 and −0.24at 820 nm for N = 4, with a subsequent decrease to −0.21 at780 nm, for N = 5 (Figure 4C,D). Considering the experimentally determined average number of N = 3.1 ± 1.2RH-GNRs per assembly, the LSPR peak position (λ = 727nm), bisignate CD peak positions (λ+ = 713 and λ− = 825 nm),and g-factor (−0.24 at 850 nm) are in close agreement to the corresponding values for N = 3 and N = 4 in the simulations.

We further explored the effects of gap distance (d) and rotation angle (α) between adjacent c-GNRs on the chiral signal by FDTD simulations. The simulated results showed that the g-factor reached a maximum value at d = 3.0−4.0 nm(Figure 4E and Figure S15A-C) and α = 20°−30° (Figure 4Fand Figure S15D-F). These values of d and α match the values determined from TEM and SEM (d = 3.2 ± 0.7 nm; α = 28.2± 8.7° for RH-GNRs, see Figure 3). We additionally simulated the chiroptical response of an assembly of achiral GNRs with the determined optimum structural parameters for c-GNRs(gap distance of 3.2 nm and rotation angle of 28.2°). The calculated near-field enhancement distribution maps show a significant electric field enhancement between

coupled c-GNRs, compared to achiral GNRs (Figure 4G), confirming that the self-matching assembly of c-GNRs leads to more efficient optical coupling. The simulated spectra (Figure 4H-J) show that the peak shape of a chiral assembly of achiral GNRs is consistent with that made of RH-GNRs, but the g-factor value is considerably smaller (−0.20 at 718 nm vs −0.35 at 842nm). In addition, our calculations predict that long-range ordered nanostructures made of c-GNRs by structural self-matching should display further enhanced g-factor values(Figure S17).

Inspired by the high g-factor of self-matching assemblies ofc-GNRs, we explored their use for the detection of relevant biomolecules, such as ATP and its derivatives (see Figure 5and Figure S18 for further details). As shown in Figure 5A,B,the corresponding CD and g-factor spectra for RH-GNR assemblies revealed an enhancement by ca. 25-fold (from 110to 2800 mdeg) and ca. 47-fold (from 0.004 to 0.186),respectively, as ATP concentration increased from 50 to 100μM. Such a large change in chiral signal is in contrast with themodest CD signal variation for pure ATP (from 0.70 to 1.7mdeg) for an increased concentration from 50 to 100 μM(Figure 5C and Figure S18). Therefore, we propose the plasmonic chiroptical detection of ATP by c-GNRs, as a significantly more sensitive method than the CD detection of pure ATP. On these promising grounds, we further explored the ATP detection limit. To this end, the c-GNR concentration was reduced from 1.0 to 0.40 nM (Figure 5D-F and FigureS19), achieving an ATP detection limit as low as 1.0 μM,which is significantly lower than that for previously reported chiroplasmonic sensors.[38] These results indicate that the detection of the chiroptical response of c-GNR assemblies isa sensitive and high-resolution method for ATP detection

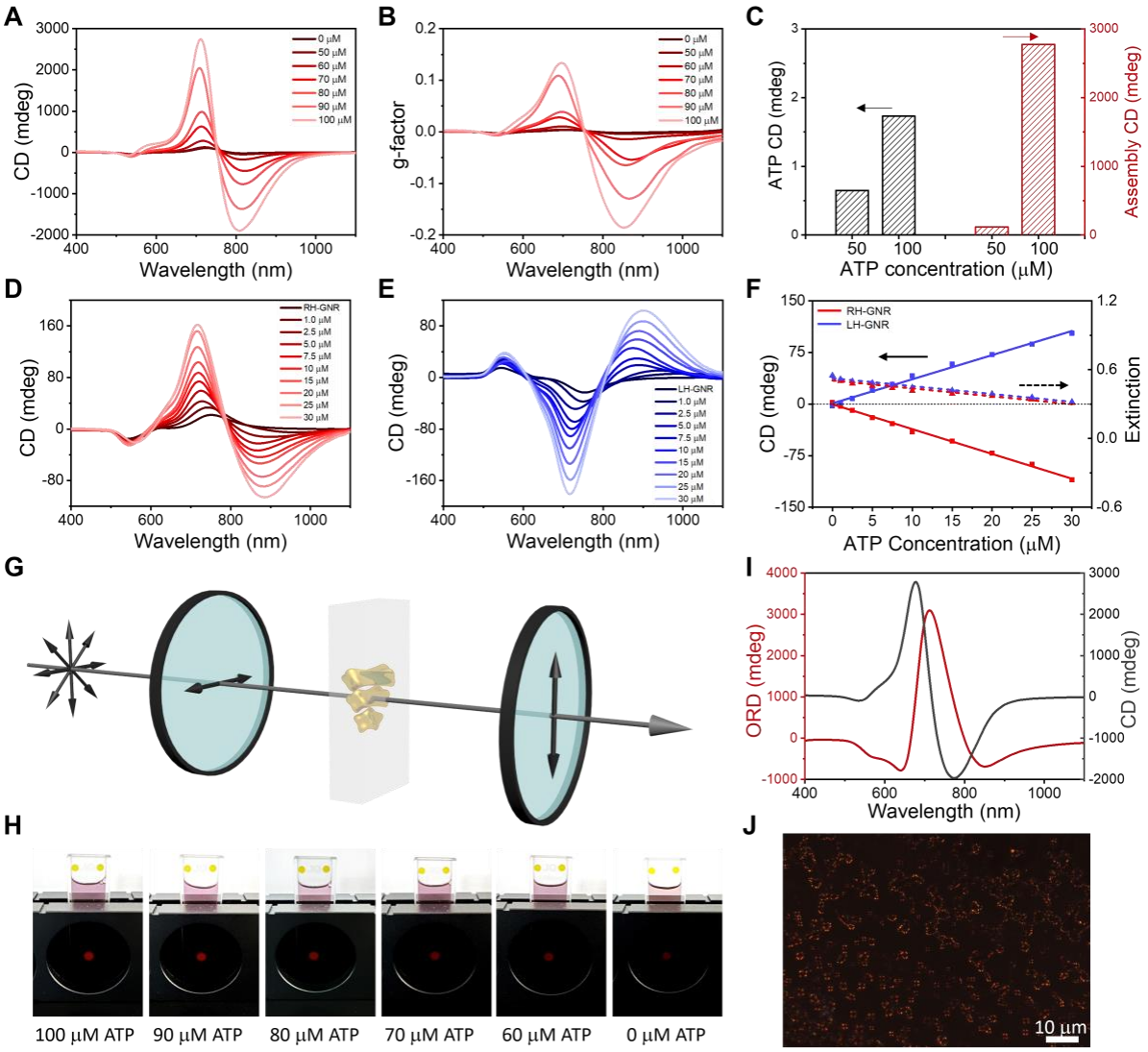

Figure 5. Detection of ATP based on c-GNR assembly. (A) CD spectra and (B) *g*-factor spectra of RH-GNR (1.0 nM) assemblies with ATP at different concentrations. (C) Maximum CD values for ATP solutions and ATP-induced assemblies of c-GNRs, for ATP concentrations of 50 and 100 μM. CD spectra of (D) RH-GNR or (E) LH-GNR (0.40 nM) assemblies after addition of ATP at different concentrations. (F) Variation of the intensity of CD at 900 nm and extinction at 750 nm, as a function of ATP concentration. Solid and dotted lines are linear fits to the data. (G) Schematics of the optical setup for polarization optical images. (H) Photographs of the RH-GNR dispersions, assembled with variable concentrations of ATP, in a cross-polarization optical cell. (I) ORD spectrum and (J) polarized optical microscopy image of RH-GNR assemblies with ATP (100 μM).

Due to the exceptionally high g-factors of c-GNR assemblies, we were able to further simplify the detection protocol by using polarization optics for naked-eye visualization of ATP detection (Figure 5G and Figure S20). As shown in Figure 5H,when RH-GNRs were assembled in the presence of ATP (60to 100 μM), strong red light could be transmitted and readily observed by eye. The transmission of red light corresponds to the strong optical rotatory dispersion (ORD) signals in the range of 600 to 800 nm (Figure 5I). In addition, high-contrast visualization of ATP and RH-GNR assemblies could also be realized by using polarized optical microscopy (Figure 5J and Figure S21), demonstrating the advantage of intense chiroptical signals for biosensing and bioimaging

ATP and its hydrolysis products, ADP and AMP, work together to regulate many biological functions and provide energy for most physiological activities.[15] Thus, it is highly desirable to detect ATP, ADP, and AMP simultaneously. We observed that ATP, ADP, and AMP with the same concentration (20 μM) induced the self-matching assembly of RH-GNRs with different optical response (Figure S22,S23). The results suggest that the achieving the simultaneous detection of ATP, ADP, and AMP by c-GNRs (Figure S24,S25 for details).

To confirm the potential application of the detection method in real samples, we further explored detection in physiological environments. The results indicate that c-GNRs can be used to detect and distinguish ATP, ADP, and AMP, both in PBS and in serum (Figures S26, S27).[59,60] These results also indicated that PBS and biomolecules in serum do not significantly interfere with ATP detection. Besides, this detection method is also applicable to the detection of drug molecules, such as sodium cromoglycate (antiallergic drug) (Figure S28), suggesting that the method based on c-GNR assembly holds promise for drug detection.

Based on their unique morphology, c-GNRs can be used as building blocks to form structural self-matching side-by-side assemblies with exceptionally high *g*-factors, up to 0.24, significantly higher than those for individual c-GNRs. The results from FDTD simulations were consistent with experimental data, showing that the mutual organization of c-GNRs within the assembly is responsible for the unusually high optical asymmetry. Furthermore, we demonstrated the sensitive detection ATP, by means of the significant enhancement of optical asymmetry. Overall, the chiral assembly of chiral NPs paves the way toward the development of chiral nanostructures with high optical asymmetry, which are relevant for applications in biosensing, chiral imaging, optoelectronic devices, etc.

ASSOCIATED CONTENT

Supporting Information.

The following files are available free of charge.

Additional data and analysis, including details on materials, experimental procedures, characterizations, equations, and additional figures.

AUTHOR INFORMATION

Corresponding Author

Luis M. Liz-Marzán - CIC biomaGUNE, Basque Research and Technology Alliance (BRTA), 20014 Donostia-San Sebastián, Spain. E-mail: llizmarzan@cicbiomagune.es

Sara Bals - EMAT and NANOlab Center of Excellence, University of Antwerp, 2020 Antwerp, Belgium. E-mail: sara.bals@uantwerpen.be

Kun Liu - State Key Laboratory of Supramolecular Structure and Materials, College of Chemistry, Jilin University, Changchun 130012, China. E-mail: kliu@jlu.edu.cn

Author Contributions

N.Z. performed the experiments. N.Z., Y.Y., T.S., L.M.L, S.B., and K.L. designed this work. M.M. performed to ET measurements. S.G., L.Y., Z.S., and S.Z. provided assistance in the experiments. L.W., Z.W., and W.Z. carried out Cryo-TEM measurements. F.P. and Z.W. contributed to SEM measurements. N.Z., M.M., L.M.L, S.B., and K.L. wrote the manuscript.

Notes

The authors declare no competing financial interest.

ACKNOWLEDGMENT

This work was financially supported by the National Natural Science Foundation of China (22225203, 22302074, 22133002, and 21975094). K.L. also thanks the JLU Science and Technology Innovative Research Team (2021TD-03). L.M.L.-M acknowledges financial support by the Spanish State Research Agency, MCIN/AEI/10.13039/501100011033 (Grant PID2020-117779RB-I00). S.B. and M.M. thank the European Research Council (ERC Consolidator Grant815128, REALNANO).

REFERENCES

(1) Wagnière, G. H. On Chirality and the Universal Asymmetry: Reflections on Image and Mirror Image; Wiley: 2007.

(2) Aggeli, A.; Nyrkova, I. A.; Bell, M.; Harding, R.; Carrick, L.; McLeish, T. C. B.; Semenov, A. N.; Boden, N. Hierarchical Self-Assembly of Chiral Rod-Like Molecules as a Model for Peptide β-sheet Tapes, Ribbons, Fibrils, and Fibers. Proc. Natl. Acad. Sci. U. S. A.2001, 98, 11857−11862.

(3) Querejeta-Fernández, A.; Hernández-Garrido, J. C.; Yang, H.; Zhou, Y.; Varela, A.; Parras, M.; Calvino-Gámez, J. J.; González-Calbet, J. M.; Green, P. F.; Kotov, N. A. Unknown Aspects of Self-Assembly of PbS Microscale Superstructures. ACS Nano 2012, 6,3800−3812.

(4) Lebreton, G.; Géminard, C.; Lapraz, F.; Pyrpassopoulos, S.;Cerezo, D.; Spéder, P.; Ostap, E.; Noselli, S. Molecular to Organismal Chirality Is Induced by the Conserved Myosin 1D. Science 2018, 362,949−952.

(5) Kumar, J.; Liz-Marzán, L. M. Recent Advances in Chiral Plasmonics: Towards Biomedical Applications. Bull. Chem. Soc. Jpn.2019, 92, 30−37.

(6) Hentschel, M.; Schäferling, M.; Duan, X.; Giessen, H.; Liu, N.Chiral plasmonics. Sci. Adv. 2017, 3, No. e1602735.

(7) Liang, J.; Guo, P.; Qin, X.; Gao, X.; Ma, K.; Zhu, X.; Jin, X.; Xu,W.; Jiang, L.; Duan, P. Hierarchically Chiral Lattice Self-Assembly Induced Circularly Polarized Luminescence. ACS Nano 2020, 14,3190−3198.

(8) Yashima, E.; Ousaka, N.; Taura, D.; Shimomura, K.; Ikai, T.;Maeda, K. Supramolecular Helical Systems: Helical Assemblies of Small Molecules, Foldamers, and Polymers with Chiral Amplification and Their Functions. Chem. Rev. 2016, 116, 13752−13990.

(9) Wang, D.; Guan, J.; Hu, J.; Bourgeois, M. R.; Odom, T. W. Manipulating Light−Matter Interactions in Plasmonic Nanoparticle Lattices. Acc. Chem. Res. 2019, 52, 2997−3007.

(10) Kuzyk, A.; Schreiber, R.; Fan, Z.; Pardatscher, G.; Roller, E.-M.;Högele, A.; Simmel, F. C.; Govorov, A. O.; Liedl, T. DNA-Based Self-Assembly of Chiral Plasmonic Nanostructures with Tailored Optical Response. Nature 2012, 483, 311−314.

(11) Smith, K. W.; Zhao, H.; Zhang, H.; Sánchez-Iglesias, A.;Grzelczak, M.; Wang, Y.; Chang, W.-S.; Nordlander, P.; Liz-Marzán, L. M.; Link, S. Chiral and Achiral Nano dumbbell Dimers: the Effect of Geometry on Plasmonic Properties. ACS Nano 2016, 10, 6180−6188.

(12) Shi, L.; Zhu, L.; Guo, J.; Zhang, L.; Shi, Y.; Zhang, Y.; Hou, K.; Zheng, Y.; Zhu, Y.; Lv, J.; Liu, S.; Tang, Z. Self-Assembly of Chiral Gold Clusters into Crystalline Nanocubes of Exceptional Optical Activity. Angew. Chem. Int. Ed. 2017, 56, 15397−15401.

(13) Wang, P.-p.; Yu, S.-J.; Govorov, A. O.; Ouyang, M. Cooperative Expression of Atomic Chirality in Inorganic Nanostructures. Nat.Commun. 2017, 8, 14312.

(14) Mokashi-Punekar, S.; Zhou, Y.; Brooks, S. C.; Rosi, N. L. Construction of Chiral, Helical Nanoparticle Superstructures: Progress and Prospects. Adv. Mater. 2020, 32, 1905975.

(15) Zhu, J.; Wu, F.; Han, Z.; Shang, Y.; Liu, F.; Yu, H.; Yu, L.; Li,N.; Ding, B. Strong Light-Matter Interactions in Chiral Plasmonic-Excitonic Systems Assembled on DNA Origami. Nano Lett. 2021, 21,3573−3580.

(16) Lu, J.; Chang, Y. X.; Zhang, N. N.; Wei, Y.; Li, A. J.; Tai, J.;Xue, Y.; Wang, Z. Y.; Yang, Y.; Zhao, L.; Lu, Z. Y.; Liu, K. Chiral Plasmonic Nanochains via the Self-Assembly of Gold Nanorods and Helical Glutathione Oligomers Facilitated by Cetyltrimethylammonium Bromide Micelles. ACS Nano 2017, 11, 3463−3475.

(17) Zhang, Q.; Hernandez, T.; Smith, K. W.; Hosseini Jebeli, S. A.;Dai, A. X.; Warning, L.; Baiyasi, R.; McCarthy, L. A.; Guo, H.; Chen,D. H.; Dionne, J. A.; Landes, C. F.; Link, S.

Unraveling the Origin of Chirality from Plasmonic Nanoparticle-Protein Complexes. Science2019, 365, 1475−1478.

(18) Wang, Z. Y.; Zhang, N. N.; Li, J. C.; Lu, J.; Zhao, L.; Fang, X.D.; Liu, K. Serum Albumins Guided Plasmonic Nanoassemblies with Opposite Chiralities. Soft Matter 2021, 17, 6298−6304.

(19) Juarez, X. G.; Freire-Fernandez, F.; Khorasani, S.; Bourgeois,M. R.; Wang, Y.; Masiello, D. J.; Schatz, G. C.; Odom, T. W. Chiral Optical Properties of Plasmonic Kagome Lattices. ACS Photonics2024, 11, 673−681.

(20) Lu, J.; Xue, Y.; Bernardino, K.; Zhang, N. N.; Gomes, W. R.; Ramesar, N. S.; Liu, S.; Hu, Z.; Sun, T.; Moura, A. F.; Kotov, N. A.; Liu, K. Enhanced Optical Asymmetry in Supramolecular Chiroplasmonic Assemblies with Long-Range Order. Science 2021, 371, 1368−1374.

(21) Du, C.; Li, Z.; Zhu, X.; Ouyang, G.; Liu, M. Hierarchically Self-Assembled Homochiral Helical Microtoroids. Nat. Nanotechnol. 2022,17, 1294−1302.

(22) Kumar, P.; Vo, T.; Cha, M.; Visheratina, A.; Kim, J.-Y.; Xu, W.; Schwartz, J.; Simon, A.; Katz, D.; Nicu, V. P.; Marino, E.; Choi, W. J.; Veksler, M.; Chen, S.; Murray, C.; Hovden, R.; Glotzer, S.; Kotov, N.A. Photonically Active Bowtie Nanoassemblies with ChiralityContinuum. Nature 2023, 615, 418−424.

(23) Wang, S.; Zheng, L.; Chen, W.; Ji, L.; Zhang, L.; Lu, W.; Fang,Z.; Guo, F.; Qi, L.; Liu, M. Helically Grooved Gold Nanoarrows: Controlled Fabrication, Superhelix and Transcribed Chiroptical Switching. CCS Chem. 2021, 3, 2473−2484.

(24) Maoz, B. M.; van der Weegen, R.; Fan, Z.; Govorov, A. O.;Ellestad, G.; Berova, N.; Meijer, E. W.; Markovich, G. Plasmonic Chiroptical Response of Silver Nanoparticles Interacting with Chiral Supramolecular Assemblies. J. Am. Chem. Soc. 2012, 134, 17807−17813.

(25) Zhang, N. N.; Sun, H. R.; Liu, S.; Xing, Y. C.; Lu, J.; Peng, F.; Han, C. L.; Wei, Z.; Sun, T.; Yang, B.; Liu, K. Gold Nanoparticle Enantiomers and Their Chiral-Morphology Dependence of Cellular Uptake. CCS Chem. 2022, 4, 660−670.

(26) Zhang, N. N.; Sun, H. R.; Xue, Y.; Peng, F.; Liu, K. Tuning the Chiral Morphology of Gold Nanoparticles with Oligomeric Gold-Glutathione Complexes. J. Phys. Chem. C 2021, 125, 10708−10715.

(27) Xu, L.; Wang, X.; Wang, W.; Sun, M.; Choi, W. J.; Kim, J. Y.; Hao, C.; Li, S.; Qu, A.; Lu, M.; Wu, X.; Colombari, F. M.; Gomes, W. R.; Blanco, A. L.; de Moura, A. F.; Guo, X.; Kuang, H.; Kotov, N. A.;Xu, C. Enantiomer-Dependent Immunological Response to Chiral Nanoparticles. Nature 2022, 601, 366−373.

(28) González-Rubio, G.; Mosquera, J.; Kumar, V.; Pedrazo-Tardajos, A.; Llombart, P.; Solís, D. M.; Lobato, I.; Noya, E. G.;Guerrero-Martínez, A.; Taboada, J. M.; Obelleiro, F.; MacDowell, L.G.; Bals, S.; Liz-Marzán, L. M. Micelle-Directed Chiral Seeded Growth on Anisotropic Gold Nanocrystals. Science 2020, 368, 1472−1477.

(29) Lee, H. E.; Ahn, H. Y.; Mun, J.; Lee, Y. Y.; Kim, M.; Cho, N.H.; Chang, K.; Kim, W. S.; Rho, J.; Nam, K. T. Amino-Acid- and Peptide-Directed Synthesis of Chiral Plasmonic Gold Nanoparticles. Nature 2018, 556, 360−365.

(30) Ni, B.; Mychinko, M.; Gómez-Graña, S.; Morales-Vidal, J.; Obelleiro-Liz, M.; Heyvaert, W.; Vila-Liarte, D.; Zhuo, X.; Albrecht, W.; Zheng, G.; González-Rubio, G.; Taboada, J. M.; Obelleiro, F.; López, N.; Pérez-Juste, J.; Pastoriza-Santos, I.; Cölfen, H.; Bals, S.; Liz-Marzán, L. M. Chiral Seeded Growth of Gold Nanorods into Fourfold Twisted Nanoparticles with Plasmonic Optical Activity. Adv.Mater. 2023, 35, 2208299.

(31) Kim, R. M.; Huh, J.-H.; Yoo, S.; Kim, T. G.; Kim, C.; Kim, H.; Han, J. H.; Cho, N. H.; Lim, Y.-C.; Im, S. W.; Im, E.; Jeong, J. R.; Lee,M. H.; Yoon, T.-Y.; Lee, H.-Y.; Park, Q.-H.; Lee, S.; Nam, K. T. Enantioselective Sensing by Collective Circular Dichroism. Nature2022, 612, 470−476.

(32) Wan, J.; Sun, L.; Sun, X.; Liu, C.; Yang, G.; Zhang, B.; Tao, Y.; Yang, Y.; Zhang, Q. Cu2+-Dominated Chirality Transfer from Chiral Molecules to Concave Chiral Au Nanoparticles. J. Am. Chem. Soc.2024, 146, 10640−10654.

(33) Tadgell, B.; Liz-Marzán, L. M. Probing Interactions between Chiral Plasmonic Nanoparticles and Biomolecules. Chem-eur J. 2023,29, No. e202301691.

(34) Suri, C. R.; Kaur, J.; Gandhi, S.; Shekhawat, G. S. Label-Free Ultra-Sensitive Detection of Atrazine Based on Nanomechanics. Nanotechnology 2008, 19, 235502.

(35) Pérez-Ruiz, T.; Martínez-Lozano, C.; Tomás, V.; Martín, J. Determination of ATP via the Photochemical Generation of Hydrogen Peroxide Using Flow Injection Luminol Chemiluminescence Detection. Anal. Bioanal. Chem. 2003, 377, 189−194.

(36) Przedborski, S.; Vila, M. MPTP: A Review of Its Mechanisms of Neurotoxicity. J. Clin. Invest. Clin. Neurosci. Res. 2001, 1, 407−418.

(37) Bush, K. T.; Keller, S. H.; Nigam, S. K. Genesis and Reversal of the Ischemic Phenotype in Epithelial Cells. J. Clin. Invest. 2000, 106,621−626.

(38) Fu, P.; Sun, M.; Xu, L.; Wu, X.; Liu, L.; Kuang, H.; Song, S.;Xu, C. A Self-Assembled Chiral-Aptasensor for ATP Activity Detection. Nanoscale 2016, 8, 15008−15015.

(39) Gilroy, C.; Hashiyada, S.; Endo, K.; Karimullah, A. S.; Barron,L. D.; Okamoto, H.; Togawa, Y.; Kadodwala, M. Roles of Superchirality and Interference in Chiral Plasmonic Biodetection. J. Phys. Chem. C 2019, 123, 15195−15203.

(40) Lee, Y. Y.; Kim, R. M.; Im, S. W.; Balamurugan, M.; Nam, K. T. Plasmonic Metamaterials for Chiral Sensing Applications. Nanoscale2020, 12, 58−66.

(41) Zhang, N. N.; Shen, Z. L.; Gao, S. Y.; Peng, F.; Cao, Z. J.; Wang, Y.; Wang, Z.; Zhang, W.; Yang, Y.; Liu, K.; Sun, T. Synthesisand Plasmonic Chiroptical Properties of Double-Helical GoldNanorod Enantiomers. Adv. Optical Mater. 2023, 11, 2203119.

(42) Heyvaert, W.; Pedrazo-Tardajos, A.; Kadu, A.; Claes, N.;González-Rubio, G.; Liz-Marzán, L. M.; Albrecht, W.; Bals, S. Quantification of the Helical Morphology of Chiral Gold Nanorods. ACS Mater. Lett. 2022, 4, 642−649.

(43) Zhang, N. N.; Shen, X.; Liu, K.; Nie, Z.; Kumacheva, E. Polymer-Tethered Nanoparticles: From Surface Engineering toDirectional Self-Assembly. Acc. Chem. Res. 2022, 55, 1503−1513.

(44) Lan, X.; Wang, Q. Self-Assembly of Chiral Plasmonic Nanostructures. Adv. Mater. 2016, 28, 10499−10507.

(45) Duan, T.; Ai, J.; Cui, X.; Feng, X.; Duan, Y.; Han, L.; Jiang, J.; Che, S. Spontaneous Chiral Self-Assembly of CdSe@CdS Nanorods. Chem. 2021, 7, 2695−2707.

(46) Nguyen, L.; Dass, M.; Ober, M. F.; Besteiro, L. V.; Wang, Z.M.; Nickel, B.; Govorov, A. O.; Liedl, T.; Heuer-Jungemann, A. Chiral Assembly of Gold-Silver Core-Shell Plasmonic Nanorods on DNA Origami with Strong Optical Activity. ACS Nano 2020, 14, 7454−7461.

(47) Jain, P. K.; Eustis, S.; El-Sayed, M. A. Plasmon Coupling in Nanorod Assemblies: Optical Absorption, Discrete Dipole Approximation Simulation, and Exciton-Coupling Model. J. Phys. Chem. B2006, 110, 18243−18253.

(48) Hou, S.; Zhang, H.; Yan, J.; Ji, Y.; Wen, T.; Liu, W.; Hu, Z.; Wu, X. Plasmonic Circular Dichroism in Side-By-Side Oligomers of Gold Nanorods: the Influence of Chiral Molecule Location and Interparticle Distance. Phys. Chem. Chem. Phys. 2015, 17, 8187−8193.

(49) Ma, W.; Kuang, H.; Wang, L.; Xu, L.; Chang, W. S.; Zhang, H.; Sun, M.; Zhu, Y.; Zhao, Y.; Liu, L.; Xu, C.; Link, S.; Kotov, N. A. Chiral plasmonics of self-assembled nanorod dimers. Sci. Rep. 2013, 3,1934.

(50) Sun, Z.; Ni, W.; Yang, Z.; Kou, X.; Li, L.; Wang, J. pH-Controlled Reversible Assembly and Disassembly of Gold Nanorods. Small 2008, 4, 1287−1292.

(51) He, Y.; Li, H.; Steiner, A. M.; Fery, A.; Zhang, Y.; Ye, C. Tunable Chiral Plasmonic Activities Enabled via Stimuli ResponsiveMicro-Origami. Adv. Mater. 2023, 35, 2303595.

(52) Gong, Y.; Cao, Z.; Zhang, Z.; Liu, R.; Zhang, F.; Wei, J.; Yang, Z. Chirality Inversion in Self-Assembled Nanocomposites Directed by Curvature-Mediated Interactions. Angew. Chem. Int. Ed. 2022, 61,No. e202117406.

(53) Wang, Y.; Chen, G.; Yang, M.; Silber, G.; Xing, S.; Tan, L. H.; Wang, F.; Feng, Y.; Liu, X.; Li, S.; Chen, H. A Systems Approach Towards the Stoichiometry-Controlled Hetero-Assembly of Nano-particles. Nat. Commun. 2010, 1, 87.

(54) Han, B.; Shi, L.; Gao, X.; Guo, J.; Hou, K.; Zheng, Y.; Tang, Z. Ultra-Stable Silica-Coated Chiral Au-Nanorod Assemblies: Core-Shell Nanostructures with Enhanced Chiroptical Properties. Nano Res.2016, 9, 451−457.

(55) Pan, J.; Wang, X.; Zhang, J.; Zhang, Q.; Wang, Q.; Zhou, C. Chirally Assembled Plasmonic Metamolecules from Intrinsically Chiral Nanoparticles. Nano Res. 2022, 15, 9447−9453.

(56) Maniappan, S.; Dutta, C.; Solís, D. M.; Taboada, J. M.; Kumar,J. Surfactant Directed Synthesis of Intrinsically Chiral Plasmonic Nanostructures and Precise Tuning of Their Optical Activity through Controlled Self-Assembly. Angew. Chem. Int. Ed. 2023, 62, No. e202300461.

(57) Yeung, P.; Ding, L.; Casley, W. L. HPLC Assay with UV Detection for Determination of RBC Purine Nucleotide Concentrations and Application for Biomarker Study in Vivo. J. Pharm. Biomed. Anal. 2008, 47, 377−382.

(58) Bian, T.; Gardin, A.; Gemen, J.; Houben, L.; Perego, C.; Lee,B.; Elad, N.; Chu, Z.; Pavan, G. M.; Klajn, R. Electrostatic Co-Assembly of Nanoparticles with Oppositely Charged Small Moleculesinto Static and Dynamic Superstructures. Nat. Chem. 2021, 13, 940−949.

(59) Gole, A.; Orendorff, C. J.; Murphy, C. J. Immobilization of Gold Nanorods onto Acid-Terminated Self-Assembled Monolayers via Electrostatic Interactions. Langmuir 2004, 20, 7117−7122.

(60) Ferhan, A. R.; Guo, L.; Kim, D. H. Influence of Ionic Strength and Surfactant Concentration on Electrostatic Surfacial Assembly of Cetyltrimethylammonium Bromide-Capped Gold Nanorods on Fully Immersed Glass. Langmuir 2010, 26, 12433−12442.